Understanding Blazar Jets
Through Their Multifrequency Emission

Rita M. Sambruna*

*Pennsylvania State University
Dept. of Astronomy & Astrophys
525 Davey Lab, University Park, PA 16802
(rms@astro.psu.edu)

Abstract.

Being dominated by non-thermal (synchrotron and inverse Compton) emission from a relativistic jet, blazars offer important clues to the structure and radiative processes in extragalactic jets. Crucial information is provided by blazars' spectral energy distributions from radio to gamma-rays (GeV and TeV energies), their trends with bolometric luminosity, and their correlated variability properties. This review is focussed on recent multiwavelength monitorings of confirmed and candidate TeV blazars and the constraints they provide for the radiative properties of the emitting particles. I also present recent observations of the newly discovered class of "blue quasars" and the implications for current blazars' unification schemes.

THE BLAZAR FAMILY

Blazars are radio-loud Active Galactic Nuclei (AGNs) with polarized, luminous, and rapidly variable non-thermal continuum emission, extending from radio to gamma-rays (GeV and TeV energies), from a relativistic jet oriented close to the line of sight. As such, they are rare laboratories to study the physics and structure of extragalactic jets, present in all radio-loud AGNs [1].

Strong clues are provided by blazars' spectral energy distributions (SEDs). These are typically double-humped (Fig. 1; from [2,3]), with the first component peaking at IR/optical wavelengths in "red blazars" (also called Low-energy peaked blazars, LBLs) and at UV/X-rays in "blue blazars" (or HBLs, High-energy peaked blazars) [1]. Its rapid variability and high polarization leave little doubt that it is due to synchrotron emission from relativistic electrons in the jet. The second spectral

---

[1] A practical way to discriminate between LBLs and HBLs is though their radio-to-X-ray spectral indices, α_{rx}, with $\alpha_{rx} > 0.8$ in LBLs and $\alpha_{rx} < 0.8$ in HBLs [4]. Flat Spectrum Radio Quasars (FSRQs) have SEDs similar to LBLs, but are more luminous and have stronger optical emission lines [5].
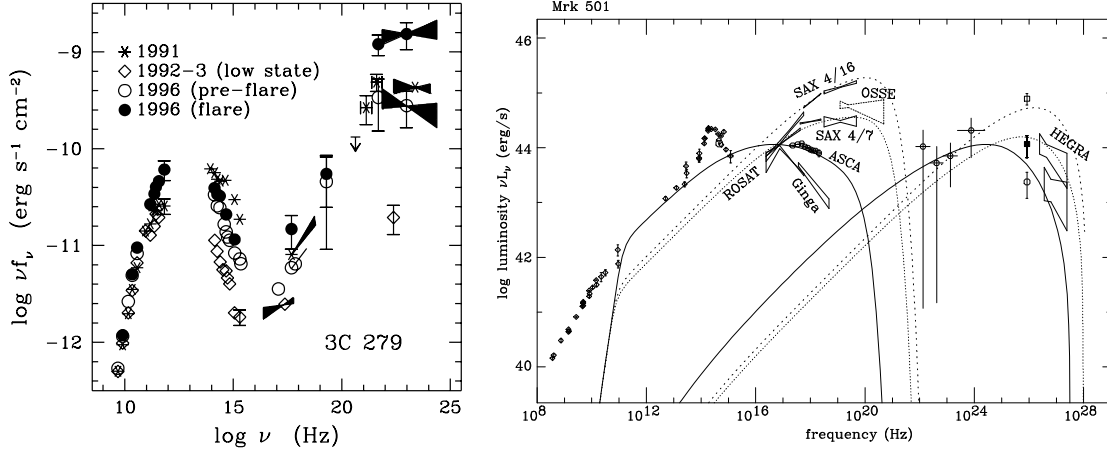
FIGURE 1. Spectral energy distributions (SEDs) of the red [Left, (a)] and blue [Right, (b):] blazars 3C 279 and Mrk 501, respectively (from [2,3]). Blazars' SEDs typically have two broad humps, the first peaking anywhere from IR/optical (in red blazars like 3C279) to hard X-rays (in blue blazars like Mrk 501) and due to synchrotron emission from a relativistic jet. The second component, extending to gamma-rays, is less well understood. A popular explanation is inverse Compton scattering of ambient seed photons off the jet's electrons. The largest variability amplitudes are observed above the peaks in both sources.

component extends from X-rays to gamma-rays, and its origin is less well understood. In the leptonic models, it could be due to inverse Compton (IC) scattering off the electrons of photons either internal or external to the jet (synchrotron-self Compton, SSC and external Compton, EC, respectively; see, e.g., [6]). Here I will assume the leptonic models, but acknowledge that an alternative is provided by the hadronic scenario (e.g., [7]).

Red and blue blazars are just the extrema of a continuous distribution of SEDs [8,9]. Indeed, deep multicolor surveys [10,11] are finding an increasing number of sources with intermediate SED shapes, and new trends with jet bolometric luminosity are discovered [8,12]. Specifically, the lower-luminosity blue blazars have higher synchrotron and IC peak frequencies, lower ratios of the IC to synchrotron peak fluxes, and weaker or absent optical emission lines than their more luminous red counterparts.

A possible interpretation is that the different SEDs are due to different predominant electrons' cooling mechanisms [13]. In a homogeneous scenario, the synchrotron peak frequency $\nu_{peak} \propto \gamma_{peak}^2$, where γ_{peak} is the electron energy determined by the competition between acceleration and cooling. Because of the lower energy densities, in line-less blue blazars the balance between heating and cooling is achieved at larger γ_{peak}. In contrast, in red blazars the electrons are more efficiently cooled due to the additional EC component and reach a lower final γ_{peak}. The emerging scenario is that blue blazars are SSC-dominated, while the EC

mechanism dominates the production of gamma-rays in red blazars. While there are a few caveats to this picture [14], the clear message is that the spectral diversity of blazars' jets cannot be explained by beaming/orientation effects *only*, but require instead a change of physical parameters and/or a different jet environment [8,15].

PROBING BLAZARS' PARADIGM: MULTIWAVELENGTH VARIABILITY OF TEV BLAZARS

Correlated multiwavelength variability provides a way to test the cooling paradigm since the various synchrotron and IC models make different predictions for the relative flare amplitudes and shape, and the time lags. Since the same population of electrons is responsible for emitting both spectral components (in a homogeneous scenario), correlated variability of the fluxes at the low- and high-energy peaks with no lags is expected (see [16] and references therein). In blue blazars, the TeV emission is largely due to lower-energy electrons scattering low-energy (IR) photons, with the higher-energy electrons ($\gamma > \gamma_{peak}$) producing the harder TeV photons [17]. The X-ray light curve should track the TeV one, with relative amplitude for the flares at the two energies in a linear relationship [18]. Thus, *TeV blazars probe the spectrum of the emitting particles.* This is amply demonstrated by the case of Mrk 421 and Mrk 501, the two brightest and best-studied TeV blazars.

Mrk 421

Mrk 421 was extensively studied during multifrequency campaigns conducted in 1994, 1995, and 1998. The early monitorings with ASCA, Whipple, EUVE, and ground-based telescopes established that the X-ray and TeV emission is well correlated on longer ($\sim$ days) timescales, with amplitude generally decreasing with increasing wavelength [19], although within a rather sparse sampling. An intensive campaign, continuous over a period of seven days, was performed in 1998 April, involving ASCA, SAX, EUVE, and various TeV telescopes [20]. The ASCA and TeV light curves are shown in Fig. 2a. Complex X-ray flux and spectral variability is detected by ASCA, with short ($\sim$ 0.5 day) flares superposed on a longer trend and intra-day variations. The TeV light curve, disrupted by unfortunate episodes of bad weather, tracks the general trend observed at X-rays.

A few days before the start of the ASCA observations and partly overlapping with it, Mrk 421 was observed with Whipple and SAX, with a strong flare observed at both wavelengths (Fig. 2b). The new and exciting result is the first detection of X-ray/TeV correlated variability on timescales of *hours* [21], strongly supporting the idea that the same electron population is responsible for emitting the X-rays
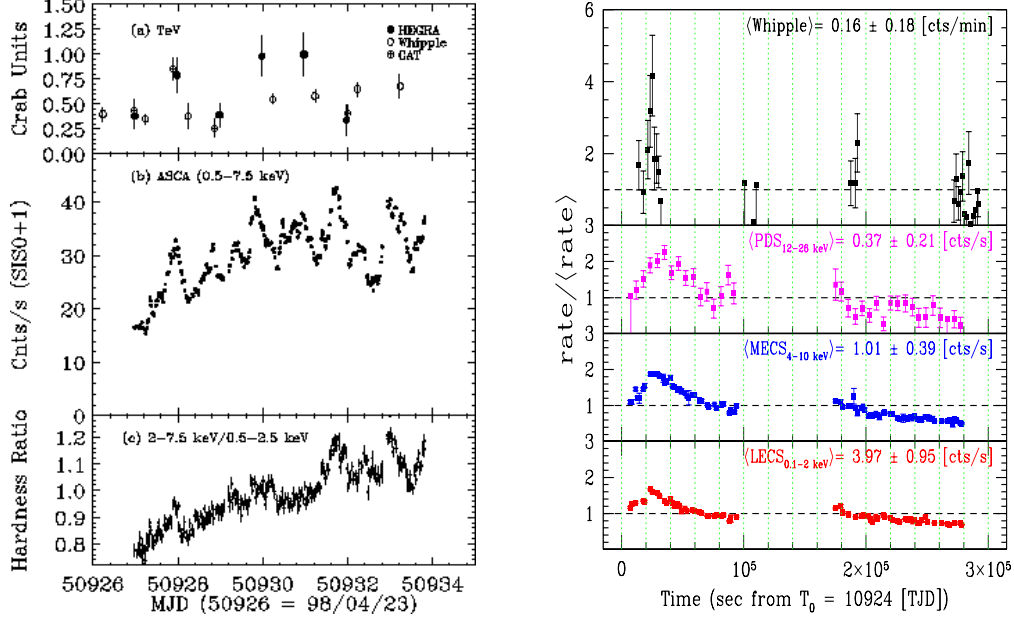
FIGURE 2. Multiwavelength observations of Mrk 421 in 1998 April. [Left, (a):] Simultaneous
TeV and X-ray continuous monitoring over a period of seven days [20]. Despite the gaps in
the sampling, the TeV light curve tracks the X-ray variations over longer ($\sim$ days) timescales.
Complex flux and spectral variations are observed at X-rays, with several short flares of $\sim$ one
day superposed over a longer trend and intra-day variations. [Right, (b):] Whipple and SAX
observations of a TeV/X-ray flare at the beginning of the 1998 April monitoring [21]. The curves
are binned at 28 minutes. Correlated X-ray and TeV flux changes on timescales of hours are
detected, strengthening the idea that the same electron population is responsible for emitting the
X-rays via synchrotron and the TeV photons via inverse Compton.

via synchrotron and the TeV photons via IC. Note the different decay times of
the flare, much faster at TeV than at X-rays (Fig. 2b), difficult to explain in the
context of a simple homogeneous model [21].

Mrk 501

Mrk 501 attracted much attention in 1997 April when it underwent a spectacular
flare at TeV energies [22–24], well correlated with a similarly-structured X-ray flare
detected by RXTE. No delays longer than one day were detected between the X-ray
and TeV emission [25]. A remarkable spectral behavior was observed in the X-rays
(Fig. 1b), where an unusually flat (photon index $\Gamma_X \sim 1.8$) X-ray continuum
was measured by SAX and RXTE during the TeV flare [26,25]. This implies a
shift of the synchrotron peak toward higher energies by more than two orders of
magnitude, almost certainly reflecting a large increase of the electron energy [26], or
the injection of a new electron population on top a quiescent one [3]. Later RXTE
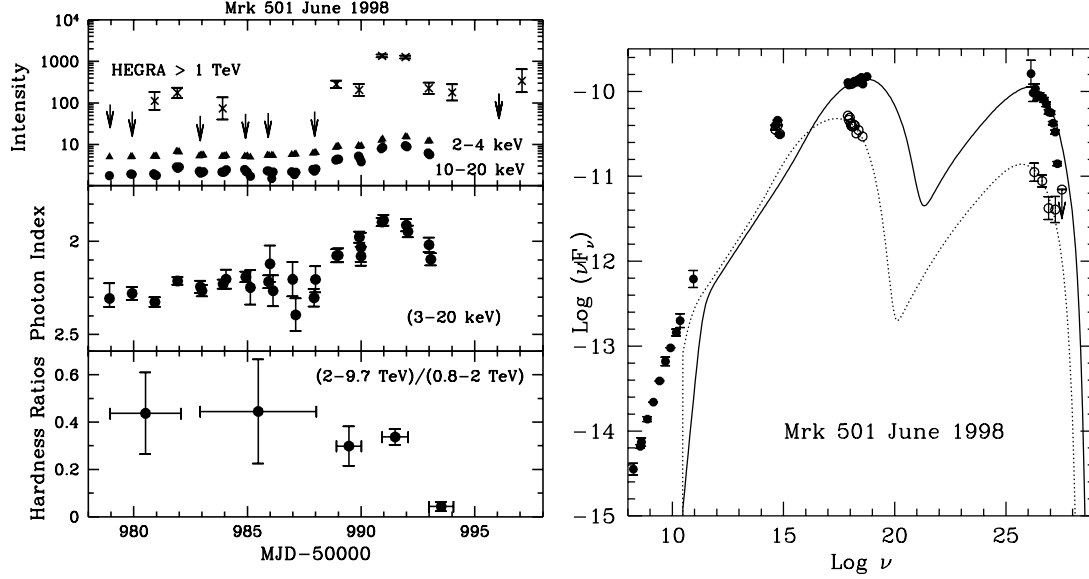
FIGURE 3. Multiwavelength campaign of Mrk 501 in 1998 June with RXTE and HEGRA [29]. [Left, (a):] TeV and X-ray light curves in different energy ranges (top panel). A large-amplitude flare is detected at TeV energies, well-correlated to a shorter-amplitude flare in the X-rays. Large X-ray spectral variations are observed (middle panel), while the TeV hardness ratios stay constant during the flare and soften one day after (bottom panel). [Right, (b):] Spectral energy distribution during the flare (filled circles) and during quiescence (open circles), fitted with the SSC model (solid and dotted lines; see [29] for details). The large spectral variability at X-rays implies a shift of the synchrotron peak at ≥ 50 keV in ~ 2 days, faster than in 1997. This indicates a similar energizing mechanism at both epochs operating on different timescales.

observations in 1997 July found the source still in a high and hard X-ray state [27], indicating a persistent energizing mechanism. A similarly flat X-ray continuum was observed in another weaker TeV blazar, 1ES2344+514 [28].

An interesting new behavior was observed during our latest 2-week RXTE and HEGRA monitoring of Mrk 501 in 1998 June [29], when 100% overlap between the X-rays and TeV light curves was achieved (Fig. 3a). A strong (factor 20 or more), short-lived ($\sim$ two days) TeV flare is detected, well correlated to a lower-amplitude, broader flare in the X-rays. As in 1997 April, large X-ray spectral variations are observed in 1998 June, with the X-ray continuum flattening to $\Gamma_X = 1.9$ at the peak of the TeV flare. This implies a similar shift to ≥ 50 keV of the synchrotron peak, but on much faster timescales (Fig. 3b). However, while in 1997 April the TeV spectrum hardened during the flare [24], as it did in the X-rays, in 1998 June the TeV hardness ratios stayed relatively constant during the flare and softened one day later (Fig. 3a). The correspondence between the X-ray and TeV spectra is no longer present during the 1998 June flare.

Intra-hour TeV variability is also detected, with a doubling timescale for the

TeV flux of $\sim$ 30 min [29]. No correlation with the X-ray light curve on such short timescales was possible, due to unfortunate gaps in the RXTE sampling. The short TeV variability timescale implies a size of the emitting region $R \leq 5 \times 10^{14}$ cm and a Doppler factor of the emitting plasma $\delta \geq 10$, similar to Mrk 421 [30].

## ACCELERATION AND COOLING IN BLAZARS JETS

Multiwavelength correlated variability of the synchrotron emission provides tight clues to the structure of the jet through the study of the energy-dependence of the flare and the accompanying spectral variations. The rise and decay times of the synchrotron flux depend on a few source typical timescales [31], while the accompany spectral variability is a strong diagnostic of the electron acceleration versus cooling processes [32], with characteristic patterns predicted for the hardness ratios as a function of total intensity depending on the timescales of the two processes. When cooling dominates, the radiative time can be approximated by the lag between the shorter and longer synchrotron wavelengths, providing an estimate of the magnetic field B of the source via $t_{lag} \sim t_{cool} \propto E^{-0.5}\delta^{-0.5}B^{-1.5}$, where E is in keV, B in Gauss, and δ is the Doppler factor of the emitting plasma [19,33].

Two excellent laboratories to study the energy propagation of the synchrotron flare are PKS 2155–304 and PKS 2005–489, since they are bright and rapidly variable at all observed wavelengths from optical to X-rays. They were the targets of recent monitorings, as described below.

Multiwavelength observations of PKS 2155–304

PKS 2155–304 was detected at TeV energies by the Durham group [34] in 1997 November, during a period of intense X-ray activity [35,36], although the source was not bright enough to allow a detailed TeV light curve. The synchrotron peak in the SED, usually in the EUV/soft X-ray energy range, shifted forward one order of magnitude [37], indicating a more modest acceleration event than in Mrk 501. Because of its intermediate SED, the correlated TeV and X-ray variability properties of PKS 2155–304 could be different than the Markarian objects, and this source qualifies as a high-priority candidate for future X-ray/TeV monitoring campaigns.

In 1991 November, PKS 2155–304 was observed with 4.5-day continuous monitoring from optical to UV and X-rays. It exhibited small-amplitude (10%), energy-*independent* variability, with well-correlated flares from optical to X-rays on timescales of a few hours and the shorter wavelengths leading the longer ones [38]. However, in a subsequent campaign in 1994 May, PKS 2155–304 showed a substantially different behavior. The source was observed continuously for $\sim$ 10 days in UV and EUV, and for 2 days in the X-rays and optical [33], exhibiting energy-*dependent* variations. A well-defined X-ray flare was observed, followed by broader, lower-amplitude flares at EUV and UV by $\sim$ 1 and 2 days, respectively. In X-rays, the harder energies lead the softer ones by one hour [39,40], implying a
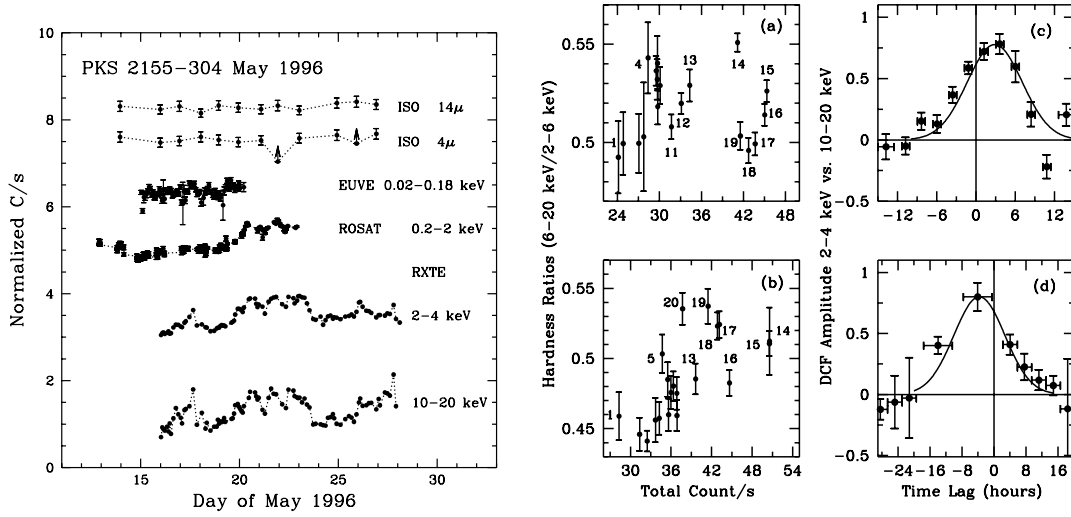
FIGURE 4. Multiwavelength monitoring of PKS 2155–304 in 1996 May [41]. [Left, (a):] Multiwavelength light curves, showing the excellent sampling at X-rays and the poorer coverage at the longer wavelengths. Complex flux and spectral variability was detected in the X-rays, with energy-dependent amplitude and different flares exhibiting different spectral behaviors in the hardness ratio versus flux diagram. Hysteresis loops of both "clockwise" and "anti-clockwise" signs are observed. [Middle, (b):] Two examples of clockwise (upper panel) and anti-clockwise (lower panel) loops for the May 18.5–20.2 and 24.2–26.9 flares, respectively. [Right, (c):] Discrete Correlation Function applied to the same flares. Soft and hard lags are detected for the clockwise and anti-clockwise loops, respectively, of $\sim$ a few hours. This complex spectral behavior is a powerful diagnostic of the acceleration and cooling processes in the jet.

magnetic field of $B \sim 0.1$ Gauss for $\delta = 10$, similar to Mrk 421 [19,33]. This apparent progression of the X-ray flare to longer wavelengths in 1994 May was explained well by an acceleration (or equivalent) event in the context of synchrotron radiation, with the time delay reflecting either synchrotron loss timescales or physical inhomogeneities of the emission region [33]. However, the quantitatively different behaviors between the campaigns in 1991 and 1994 show that the variability properties of blazars are complex, involving different modes and likely reflecting an underlying complexity in the jet structure and/or in the emission mechanisms.

PKS 2155–304 was monitored again in 1996 May from IR to X-rays (Fig. 4a; from [41]). In the X-rays excellent sampling was achieved with RXTE, and a complex flux and spectral behavior was observed, with short ($\sim$ 1-2 days), energy-dependent flares superposed to a longer-timescale trend. Inspection of the X-ray hardness ratios versus flux shows that the individual flares exhibit different spectral variability patterns. Hysteresis loops of opposite signs, both in a "clockwise" (C) and "anti-clockwise" (A) sense, are observed (Fig. 4b,c). Analysis of individual flares with various correlation methods shows that C loops correspond to soft lags (hard energies varying first) while A loops correspond to hard lags (soft energies
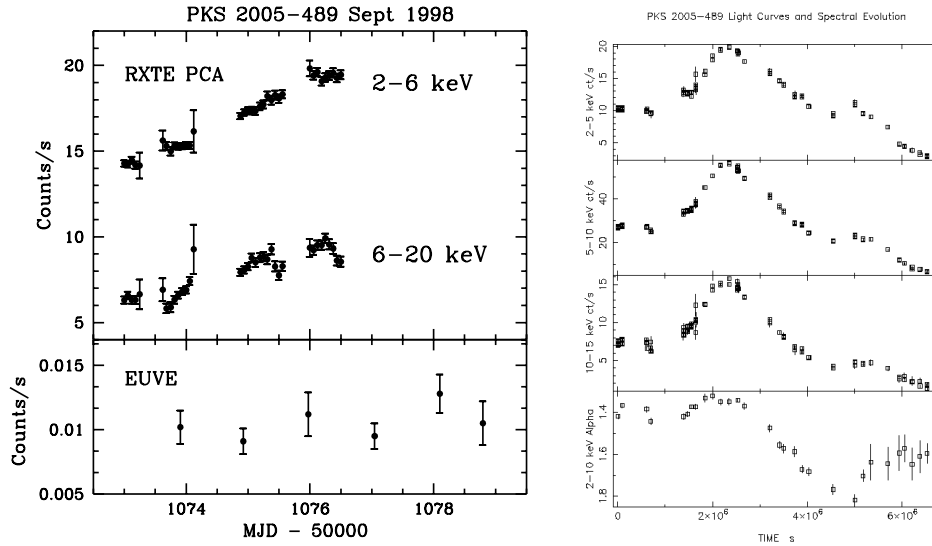
FIGURE 5. Multiwavelength observations of the TeV candidate PKS 2005–489. [Left, (a):] Our RXTE and EUVE monitoring in 1998 September. At EUV energies, the source was too faint and no variability is observed in the daily-binned light curve. Despite the gaps in the RXTE sampling, energy-dependent variability is apparent at X-rays, with a general flux increase of 30% or more in amplitude. The harder energies vary before the softer ones, consistent with cooling dominating the flux variability. [Right, (b):] One month later, PKS 2005–489 underwent a strong, long-lasting X-ray flare which was well sampled by RXTE, exhibiting spectral variations on timescales of hours [45], with similar variability patterns as in 1998 September.

varying first).

This behavior is consistent with a model where energetic electrons are injected in the source via a shock and escape into the emission region, where they cool [32]. When acceleration is faster than cooling, the latter dominates variability and, because of its energy dependence, the harder energies are emitted first, with C loops/soft lags observed. If instead the acceleration is slower ($t_{acc} \sim t_{cool}$), the electrons need to work their way up in energy and the softer energies are emitted first, yielding A loops and hard lags. For the first time, we are observing electron acceleration, which, together with cooling, is responsible for the observed X-ray variability properties of PKS 2155–304 in 1996 May.

The TeV candidate PKS 2005–489

PKS 2005–489 qualifies as a TeV candidate because of its SED, similar to Mrk 421, and its proximity (z=0.071) [42,43]. Observations by the CANGAROO group yielded only an upper limit to the TeV flux [44]. We monitored this source in 1998 September with RXTE and EUVE, to study the energy-dependence of the
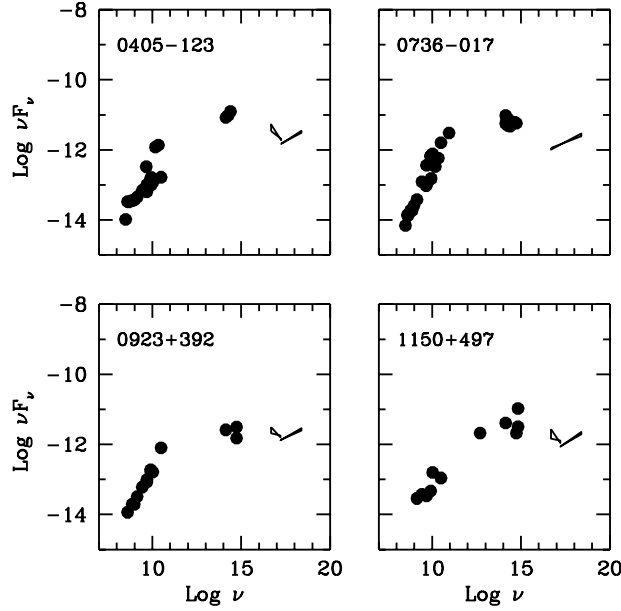
FIGURE 6. Spectral energy distributions of four blue quasars, from our recent ASCA observations and archival ROSAT and longer-wavelength data [48]. The ASCA continua are flat, implying an upturn at energies > 2 keV. The nature of the optical-to-soft X-ray emission is not well constrained, and both a thermal (from the accretion disk) and non-thermal (synchrotron emission from the jet) origin is possible. It is important to discriminate between these two scenarios with future observations, since a non-thermal origin would represent a challenge for current blazar unification schemes.

synchrotron flares. Unfortunately, the source was faint at EUV wavelengths, with a count rate of ~ 0.01 c/s; no variability is observed in the daily-binned light curve (Fig. 5a). The X-ray light curves in a soft (2–6 keV) and hard (6–20 keV) energy band are shown in Fig. 5a. Despite the gaps, due to the RXTE observational constraints, it is apparent that the variability at hard X-rays is faster than at soft X-rays, consistent with cooling dominating the synchrotron flux changes. This is confirmed by the analysis of the hardness ratios versus flux, where only clockwise loops are observed. A similar behavior was also observed one month later during a larger-amplitude, longer-lasting flare, when spectral variations occurred on timescales of a few hours [45] (Fig. 5b).

BLUE QUASARS:
UNDERMINING THE BLAZAR PARADIGM?

A simple and yet powerful probe of the blazar paradigm described above is provided by the X-ray spectra of the various blazar classes. In blue blazars, where the synchrotron peak falls at high frequencies, the X-rays are dominated by the high-

energy tail of the synchrotron component and their X-ray continua should thus be steep and convex, as a result of radiative losses. On the other end of the spectral sequence, FSRQs are dominated in the X-rays by the emerging Compton component and their X-ray continua should be flatter. This is confirmed by observations of large samples of sources with ROSAT and ASCA [9,46], which yield flat (photon index $\Gamma_X \sim 1.5$) X-ray continua for FSRQs, steep ($\Gamma_X \sim 2.5$) and downward-curved continua for HBLs, and intermediate slopes for LBLs ($\Gamma_X \sim 2.0$).

It was thus surprising when a sub-group of FSRQs, with otherwise "canonical" properties, was observed to have unusually steep ROSAT spectra, $\Gamma_{0.1-2.4\ keV} > 2$, similar to HBLs [9,47]. These objects were dubbed "blue quasars" to indicate that they could be the quasar counterparts of HBLs, contrary to the predictions of the blazar paradigm which purports that blue blazars are essentially line-less. Recent deep multicolor surveys, including our own [10], are finding an increasing number of these sources, which now amount to a non-negligible fraction of the total blazar population.

What is the true nature of blue quasars? A first simple test is to measure their hard X-ray continua. If synchrotron dominates the optical through X-ray emission, as in HBLs, the X-ray emission above 2 keV should be as steep or even steeper than at softer energies. We performed exploratory ASCA observations of four blue quasars from our ROSAT sample [9], selected because relatively nearby ($z < 1$) and *not* yet detected at gamma-rays, thus avoiding an *a priori* bias toward flat X-ray slopes. We find that their ASCA spectra are consistent with flat X-ray continua above 2 keV, $\Gamma_{2-10\ keV} \sim 1.5$, similar to the "canonical" FSRQs of the red type and implying an upturn in the SEDs (Fig. 6), most likely the onset of the Compton tail [48].

In Fig. 6, the nature of the emission below 1 keV is not well constrained, and both a thermal and non-thermal origin is possible. To this regard, blue quasars could be similar to 3C 273 and 3C 345, two quasar-like blazars where a thermal "blue bump" from the accretion disk is notoriously present, intruding into the soft X-rays (see [9] and references therein). It is thus entirely plausible that the large α_{rx} observed in blue blazars (or at least some of them) is due to a strong thermal contribution from the accretion disk, as in 3C 273 and 3C 345. Future simultaneous optical-UV-X-ray spectra will have the potential to better constrain the nature of blue quasars and their role in the blazar family.

CONCLUSIONS AND FUTURE PROSPECTS

Recent multiwavelength campaigns of blazars expanded the currently available database, from which we are learning important new lessons. Detailed modeling of the SEDs of bright gamma-ray blazars of the red and blue types tend to support the current cooling paradigm, where the different blazars flavors are related to the predominant cooling mechanisms of the electrons at the higher energies (EC in more luminous red sources, SSC in lower-luminosity blue ones). Future larger

statistical samples are needed, to fully address the observational biases, especially in gamma-rays. In particular, it will be important to expand the sample of TeV blazars, which currently includes only a handful of sources.

Correlated multiwavelength variability is the key to understanding the structure of blazars' jets. In TeV blazars, the X-rays are well correlated to the TeV emission down to timescales of days and hours (in Mrk 421), supporting a model where the same electrons are responsible for the emission at both wavelengths. It will be important to determine the shortest timescales on which this correlation holds, to pin down the electron energy distribution and the location of the emitting region(s) in the jet. This awaits well-sampled gamma-ray light curves, which will be afforded by the next higher-sensitivity missions (HESS, VERITAS, MAGIC, CANGAROO II at TeV and GLAST at GeV). Broader-band, higher quality gamma-ray spectra will also be available, allowing a more precise location of the Compton peak.

An outstanding still unanswered question is the jet composition (electrons/positrons versus protons). Single-epoch SEDs of blazars are adequately modeled by both the leptonic and hadronic models, with different tuning of the parameters. However, while the leptonic models make specific predictions for the correlated variability properties, more extensive modeling is currently needed in the context of the proton jet models. A first effort was presented at this meeting [7].

Finally, coordinated X-ray and longer-wavelength observations of the synchrotron component in blue blazars strongly suggests that acceleration, cooling, and escape are the dominant mechanisms responsible for the observed variability properties. The case of PKS 2155–304 shows that different flaring modes could be present in a single source, stressing the importance of multi-epoch monitorings to obtain a complete picture of the physical processes in blazar jets.

REFERENCES

1. Urry, C.M. and Padovani, P., *PASP* **10**, 803 (1995).
2. Wehrle, A. et al. *ApJ* **497**, 178 (1998).
3. Kataoka, J. et al., *ApJ* **514**, 138 (1999).
4. Padovani, P. and Giommi, P., *ApJ* **444**, 567 (1995).
5. Scarpa, R. and Falomo, R., *A&A* **325**, 109 (1997).
6. Böttcher, M. (1999), this volume.
7. Rachen, J. (1999), this volume.
8. Sambruna, R.M., Maraschi, L., and Urry, C.M., *ApJ* **463**, 444 (1996).

9. Sambruna, R.M. *ApJ* **487**, 536 (1997).

10. Perlman, E.S. (1999), this volume.

11. Laurent-Muehleisen, S. et al., *ApJS* **118**, 127 (1998).

12. Fossati, G. et al., *MNRAS* **299**, 433 (1998).

13. Ghisellini, G. et al., *MNRAS* **301**, 451 (1998).

14. Urry, C.M., *Astroparticle Physics* **11**, 159 (1999).

15. Georganopoulos, M. and Marscher, A., *ApJ* **506**, 621 (1998).

16. Sambruna, R.M., "Coordinated RXTE and multiwavelength observations of blazars", in *Proceedings of the Frascati '99 Workshop on Multifrequency behavior of high-energy cosmic sources*, May 24–29, Vulcano, Italy, MEMSAIt (1999) in press.

17. Tavecchio, F., Maraschi, L., & Ghisellini, G., *ApJ* **509**, 608 (1998).

18. Coppi, P. and Aharonian, F., *ApJ* **521**, L33 (1999).

19. Takahashi, T. et al., *ApJ* **470**, L89 (1996).

20. Takahashi, T. et al., *Astroparticle Physics* **11**, 177 (1999).

21. Maraschi, L. et al., *ApJ Letters* (1999), in press.

22. Catanese, M. et al., *ApJ* **487**, 143 (1997).

23. Aharonian, F. et al., *A&A* **342**, 69 (1999).

24. Djannati-Atai, A. et al., *A&A* (1999) in press (astro-ph/9906060).

25. Krawczynski, H. et al., *A&A* (1999), in press.

26. Pian, E. et al. *ApJ* **486**, 770 (1998).

27. Lamer, G. and Wagner, S. *A&AL* **331**, 13 (1998).

28. Giommi, P., Padovani, P. and Perlman, E.S., *MNRAS*, in press (1999) (astro-ph/9907377).

29. Sambruna, R.M. et al., *ApJ Letters* (1999), subm.

30. Gaidos, J.A. et al., *Nature* **383**, 319 (1996).

31. Chiaberge, M. and Ghisellini, G., *MNRAS* **306**, 551 (1999).

32. Kirk, J.G., Riegler, F.M., and Mastichiadis, A., *A&A* **333**, 452 (1998).

33. Urry, C.M. et al. *ApJ* **486**, 799 (1997).

34. Chadwick, P. et al., *ApJ* **513**, 161 (1999).

35. Chiappetti, L. et al., *ApJ* **521**, 552 (1999).

36. Chadwick, P. et al. (1999), this volume.

37. Bertone, E. et al. (1999), in prep.

38. Edelson, R.A. et al., *ApJ* **438**, 120 (1995).

39. Kataoka, J. et al., *ApJ* (1999), in press.

40. Zhang, Y.H. et al. *ApJ* (1999), in press (astro-ph/9907325).

41. Sambruna, R.M. et al., (1999) in prep.

42. Sambruna, R.M. et al., *ApJ* **449**, 567 (1995).

43. Stecker, F.A., De Jager, O.C., and Salamon, M.H., *ApJ* **473**, L75 (1996).

44. Roberts, M.D. et al., *A&A* **343**, 691 (1999).

45. Perlman, E.S. et al., *ApJ* **523**, L11 (1999).

46. Kubo, H. et al., *ApJ* **504**, 693 (1998).

47. Padovani, P., Giommi, P., and Fiore, F., *MNRAS* **284**, 569 (1997).

48. Sambruna, R.M., Chou, L., and Urry, C.M., *ApJ* (1999), subm.